Hydroclimatic shifts in northeast Thailand during the last two millennia - the record of Lake Pa Kho

Chawchai, S., Chabangborn, A., Fritz, S., Väliranta, M., Mörth, C-M., Blaauw, M., Reimer, P. J., Krusic, P. J., Löwemark, L., & Wohlfarth, B. (2015). Hydroclimatic shifts in northeast Thailand during the last two millennia - the record of Lake Pa Kho. *Quaternary Science Reviews*, *111*, 62-71. https://doi.org/10.1016/j.quascirev.2015.01.007

Published in:
Quaternary Science Reviews

Document Version:
Peer reviewed version

Hydroclimatic shifts in northeast Thailand during the last two millennia – the record of Lake Pa Kho

Sakonvan Chawchai[*1], Akkaneewut Chabangborn[1, 2], Sherilyn Fritz[3], Minna Väliranta[4], Carl-Magnus Mörth[1], Maarten Blaauw[5], Paula J. Reimer[5], Paul J. Krusic[6], Ludvig Löwemark[7] & Barbara Wohlfarth[*1]

[1]*Department of Geological Sciences, Stockholm University, Stockholm 10691, Sweden*

[2]*Department of Geology, the Faculty of Science, Chulalongkorn University, Bangkok 10330, Thailand*

[3]*Department of Earth and Atmospheric Sciences and School of Biological Sciences, University of Nebraska-Lincoln 68588-0340, USA*

[4]*Department of Environmental Sciences, University of Helsinki, Helsinki 4603, Finland*

[5]*Centre for Climate, the Environment & Chronology (14CHRONO), School of Geography, Archaeology and Palaeoecology, Queen's University of Belfast, Belfast BT7 1NN, UK*

[6]*Department of Physical Geography and Quaternary Geology, Stockholm University, Stockholm 10691, Sweden*

[7]*Department of Geosciences, National Taiwan University, Taipei 106, Taiwan*

[*]Corresponding Authors: Sakonvan Chawchai and Barbara Wohlfarth

Department of Geological Sciences, Stockholm University, Stockholm 10691, Sweden

E-mail: sakonvan.chawchai@geo.su.se; barbara.wohlfarth@geo.su.se

ABSTRACT

The Southeast Asian mainland is located in the central path of the Asian summer monsoon, a region where paleoclimatic data are still sparse. Here we present a multi-proxy (TOC, C/N, $\delta^{13}C$, biogenic silica, and XRF elemental data) study of a 1.5 m sediment/peat sequence from Lake Pa Kho, northeast Thailand, which is supported by 20 AMS ^{14}C ages. Hydroclimatic reconstructions for Pa Kho suggest a strengthened summer monsoon between BC 170 - AD 370, AD 800-960, and after AD 1450; and a weakening of the summer monsoon between AD 370-800, and AD 1300-1450. Increased run-off and a higher nutrient supply after AD 1700 can be linked to agricultural intensification and land-use changes in the region. This study fills an important gap in data coverage with respect to summer monsoon variability over Southeast Asia during the past 2000 years and enables the mean position of the Intertropical Convergence Zone (ITCZ) to be inferred based on comparisons with other regional studies. Intervals of strengthened/weaker summer monsoon rainfall suggest that the mean position of the ITCZ was located as far north as 35°N between BC 170-AD 370 and AD 800-960, whereas it likely did not reach above 17°N during the drought intervals of AD 370-800 and AD 1300-1450. The spatial pattern of rainfall variation seems to have changed after AD 1450, when the inferred moisture history for Pa Kho indicates a more southerly location of the mean position of the summer ITCZ.

Key words:

Wetland/peatland; geochemistry; paleoclimate; last two millennia; Asian Monsoon

Highlights

- New high-resolution ^{14}C-dated, multi-proxy peat sequence from NE Thailand
- Reconstruction of hydroclimatic variability during the past 2000 years
- Strengthened Asian summer monsoon BC 170-AD 370 and AD 800-970
- Weaker Asian summer monsoon AD 370-800 and AD 1300-1450
- Shifts in the mean position of the summer ITCZ during the past 2000 years

1. Introduction

The Asian summer monsoon during the past 2000 years was generally weaker than in the early Holocene in response to the long-term decline in summer insolation (Y. Wang et al., 2005). Yet high-resolution tree ring (Cook et al., 2010), marine (Anderson et al., 2002; Newton et al., 2006; Oppo et al., 2009), coral (Cobb et al., 2003), speleothem (Sinha et al., 2011a; Zhang et al., 2008), and lake (Yancheva et al., 2007) studies show that substantial decadal to centennial variations in summer monsoon intensity were superimposed on the long-term trend. Various hypotheses have been brought forward to explain this decadal to centennial scale variability, including solar forcing (Zhang et al., 2008); El Niño Southern Oscillation (ENSO) (Cobb et al., 2003; Mann et al., 2009) and Indo-Pacific climate variability (Prasad et al., 2014; Ummenhofer et al., 2013); movement of the mean position of the Intertropical Convergence Zone (ITCZ) (Newton et al., 2006; Sachs et al., 2009; Tierney et al., 2010); and changes in the Indian Ocean Dipole (Ding et al., 2010; Ummenhofer et al., 2013) and Pacific Walker Circulation (Yan et al., 2011).

The most detailed reconstructions of decadal and sub-decadal shifts in summer monsoon strength are derived from the network of Asian tree ring sites (MADA) extending back through the last millennium (Cook et al., 2010; Pages 2K Consortium, 2013). MADA and key speleothem records from China and India suggest, for example, a general weakening of the summer monsoon between AD 1400–1800 and a link between intense droughts during the 14th and 15th centuries and the demise of ancient societies in various parts of Asia (Buckley et al., 2010, 2014; Sinha et al., 2011b; Zhang et al., 2008).

The Asian monsoon system is comprised of several sub-systems whose modern interactions are complex, with considerable spatial variation in monsoon intensity and frequency (P. Wang et al., 2005; Wang, 2009). The Indian, the East Asian, and the Western North Pacific summer

78 monsoon subsystems influence the Southeast Asian mainland, but how these systems
79 interacted to affect the spatial pattern of past drought is not well resolved. Tree ring records
80 generally span less than 1000 years and have gaps in spatial coverage, and other
81 palaeoenvironmental data for the Southeast Asian mainland are still sparse. Thus, additional
82 regional records are critical to fully resolve spatial patterns of Asian monsoon variation during
83 the late Holocene, a key step in understanding long-term monsoon dynamics and potential
84 monsoon responses to changing global climate conditions.
85 Here we develop a high-resolution palaeoenvironmental data series (TOC, C/N, $\delta^{13}C$,
86 biogenic silica, and XRF elemental data) supported by 20 accelerator mass spectrometer
87 (AMS) ^{14}C ages, from a 1.5 m long sediment/peat sequence from Lake Pa Kho in northeast
88 Thailand (Fig. 1A). The site is located close to the present boundary between the East Asian
89 and Indian Ocean monsoon domains at 105°E (P. Wang et al., 2005), and is affected by the
90 seasonal migration of the summer monsoon and of the ITCZ.

91

92 **2.1 Regional setting**

93 Lake Pa Kho (17° 06′ N, 102° 56′ E; 175 m above sea level; <3 km^2) is presently a dammed
94 lake that flooded a former wetland (Penny, 2001). Several dams (built between 1989 and
95 2004) divide the lake into three sub-basins of different size (Fig. 1B). Low hills to the west
96 and south rise to ~230 m above sea level (Fig. 1B) and are the source of small seasonal
97 streams that feed neighboring Lake Kumphawapi. The flat area surrounding the lake is
98 primarily used as paddy fields, and for sugar cane and *Eucalyptus* plantations. The bedrock
99 underlying the alluvial sediments is mainly composed of Cretaceous and Neogene sand and
100 siltstones (El Tabakh et al., 2003; Wannakomol, 2005).

Climate in the region is tropical monsoonal, with mean air temperatures of ~22° to 25°C from November to February and 27° to 30°C from March to October (Fig. 1C). Mean annual precipitation is ~1455 mm, 88% of which falls from May to October. Thailand's tropical/subtropical monsoon shows a strong correlation with indices of the Indian summer monsoon and the Western North Pacific summer monsoon during the instrumental period (Limsakul et al., 2011). From 1980 to 2011, subdecadal and decadal weakening of the summer monsoon in Thailand has also been associated with ENSO variability, specifically with the increasing number of El Niño events (Bridhikitti, 2013; Hsu et al., 2014; Singhrattna et al., 2005).

Prior reconstructions of the regional paleoenvironment based on pollen and spore studies from a 2.30 m long sequence of Lake Pa Kho (Penny 1998, 2001) showed vegetation changes at the Pleistocene/Holocene transition (ca. 12000-10000 cal yr BP), with the expansion of tropical and sub-tropical broad-leaf taxa in response to the development of relatively humid climatic conditions (Penny, 2001, 1998). However, this reconstruction (Penny 1998, 2001) did not extend into the late Holocene and did not provide information on hydoclimatic conditions and vegetation change after 5000 cal yr BP. The absence of late-Holocene sediments suggests that the earlier coring location either did not accumulate or did not preserve the most recent history of the site.

3. Materials and methods

During fieldwork in January 2010, two overlapping 10-m long sequences were cored in the central part of the southern basin (Fig. 1B) using a modified Russian corer (7.5 cm diameter, 1 m length). The core sections were described in the laboratory, and each 1-m-long core segment was scanned with the Itrax XRF core scanner at 5 mm resolution using a Mo tube set at 30 kV and 30 mA for 60 sec/point. Distinct lithological markers and ITRAX scanning

125 results were used to correlate between parallel core segments, thus creating a composite
126 stratigraphy for coring point CP3. The sequence of 2.00-3.50 meter depth below the water
127 surface is the focus of this study and was subdivided into five lithostratigraphic units (Table
128 1). Consecutive samples comprising 1-cm intervals were freeze-dried. The part between 3.50
129 and 11.00 m depth is still being analyzed (Chabangborn, 2014).

130 Selected elemental data (Si, K, and Ti) obtained from XRF scanning were averaged over 1 cm
131 intervals and then normalized by (incoherent + coherent) scattering to remove various
132 instrumental effects (Kylander et al., 2011). Si, K and Ti are here used as proxies for mineral
133 input.

134 For further geochemical analyses, each freeze-dried and ground sample (150 samples in total)
135 was weighed into a tin capsule for analysis with an elemental analyzer (Carlo Erba NC2500)
136 connected to a Finnigan MAT Delta+ mass spectrometer. Total organic carbon (TOC) and
137 total nitrogen (TN) were measured in weight percentage, and their values are interpreted as
138 productivity indicators. C/N ratios are expressed as atomic ratios. In lake sediments these
139 ratios allow discrimination between aquatic and terrestrial organic matter sources (Meyer and
140 Teranes, 2001; Meyers, 2003). In peatlands, however, C/N ratios may indicate changes in the
141 type of peat-forming plants (Kuhry and Vitt, 1996) and/or are an indicator of the degree of
142 peat decomposition (Chimner and Ewel, 2005). $\delta^{13}C_{org}$ values are reported in parts per
143 thousand (permill, ‰) relative to the Vienna PeeDee Belemnite (VPDB, for C), with an
144 analytical error of ±0.15‰, and are here used as a proxy for the contribution of aquatic versus
145 terrestrial plants (Meyer and Teranes, 2001; Meyers, 2003).

146 To assess the productivity of siliceous microfossils, 51 samples were selected for analysis of
147 biogenic silica (BSi) and pre-cleaned with H_2O_2 and HCl to remove organic matter and
148 carbonate. The BSi content was determined by alkaline extraction of 30 mg of material in 40

149 mL of 1% Na_2CO_3 solution over a 5 hour period, with sub-samples taken at 3 (within), 4 and
150 5 hours and neutralized with 0.21N HCl. The extracts were analyzed for dissolved silica (DSi)
151 by ICP-OES (Varian Vista Ax), and the concentration data were plotted against depth/time.
152 The easily soluble phases (e.g. diatom frustules, phytoliths) are dissolved within two hours.
153 Crystalline phases (silicate minerals) take a longer time to dissolve. Through calculating a
154 linear regression between the 3, 4 and 5 hour measurements of DSi values, we can
155 differentiate the biogenic silica dissolved. The value where the linear regression crosses the
156 vertical axis (the y-intercept) of the sub-sample plots was considered to be the BSi (wt %)
157 corrected for a simultaneous dissolution of silica from minerals. Based on peaks in the BSi
158 curve, 15 sub-samples were further analyzed to estimate the relative contribution of diatoms
159 and phytoliths. Much of the sample material had however already been used for other
160 analyses; therefore the diatom/phytolith analyses are not continuous. Sub-samples for diatom
161 and phytolith analysis were treated with 10% HCl to remove any carbonates and heated in
162 H_2O_2 to oxidize organic matter. An aliquot of each sample was dried onto a cover slip, which
163 was mounted onto a glass slide using a permanent mounting medium (Zrax or Naphrax).

164 The chronostratigraphy is based on 20 AMS ^{14}C ages (Table 2; Fig. 2B, C). Sieve remains
165 (mesh size 0.5 mm) of the samples were identified under a stereomicroscope and rinsed
166 multiple times in deionized water. Samples with a sufficient amount of plant remains
167 (charcoal, seeds, leaves, insects, and small wood fragments) were chosen for dating. The
168 selected samples were dried overnight at 105ºC in pre-cleaned glass vials and sent to the
169 ^{14}CHRONO Centre at Queen's University, Belfast for analysis. The sieve residues of 9
170 samples were further examined for macroscopic plant remains and charcoal. The plant
171 assemblage types were described, and the depositional environment was classified as
172 aquatic/open water, telmatic (larger plant fragments originating from e.g. reeds, sedges and
173 horsetails), or terrestrial (Table 1, Fig. 3).

174 The radiocarbon age and one standard deviation were calculated using the Libby half-life of
175 5568 years and a fractionation correction based on $\delta^{13}C$ measured on the AMS (Table 2). The
176 age-model was constructed using Bacon, a Bayesian statistics-based routine that models
177 accumulation rates by dividing a sequence into many thin segments and estimating the (linear)
178 accumulation rate for each segment based on the (calibrated) ^{14}C dates, together with
179 assumptions about accumulation rate and its variability between neighboring segments
180 (Blaauw and Christen, 2011). Prior to selecting the present age models (CP3_82,
181 CP3_82_hiatus) (Fig. 2B, C), multiple model runs were performed using different
182 assumptions and parameters.

183

184 **4. Results**

185 4.1. Chronology

186 The ^{14}C dates for CP3 plot sequentially according to depth, but two ^{14}C dates (UBA-19841 at
187 3.40-3.44 m and UBA-23312 at 2.78-2.83 m) have older ages than expected (Table 2, Fig. 2B,
188 C) and are treated as outliers by Bacon. Sequential samples UBA-14636 (2.66-2.63 m) and
189 UBA-19839 (2.63-2.60 m) differ in age by c. 460 calibrated ^{14}C years (Table 2). Explanations
190 for this age difference between adjoining levels include low accumulation rates or the
191 presence of a hiatus. The stratigraphy, TOC, C/N ratio, elemental data and plant macrofossil
192 composition give no indication for an abrupt change or a hiatus at 2.63 m depth, but $\delta^{13}C$ and
193 BSi values show a distinct shift (Table 1, Fig. 3).

194 We therefore constructed two age models; one assuming low accumulation rates (CP3_82)
195 around 2.63 m, and one assuming the presence of a hiatus (CP3_82_hiatus) (Fig. 2B, C). Both
196 age models provide similar ages for the sequence below 2.68 m depth and above 2.63 m

depth, but result in a different duration (510 and 170 years, respectively) for the depth interval between 2.68 and 2.63 m. Lower accumulation rates between 2.68 and 2.63 m (AD 840-1320) as shown in the age model of CP3-82 (Fig. 2B) are inconsistent with the deposition of fibrous and less decomposed peat. The $\delta^{13}C_{org}$ values of -22 to 23‰ and occurrence of aquatic-telmatic plants also suggest the availability of water and conditions favorable for peat accumulation (Fig. 3). Age model CP3_82_hiatus on the other hand implies continuous accumulation between 2.68 and 2.63 m depth (AD 800-970), followed by a 330 year long hiatus (Fig. 2 C). Since peat accumulation below and above 2.63 m depth occurred at a similar rate in both age models, a sudden slowdown in accumulation rate between 2.68 and 2.63 m, at the same time as $\delta^{13}C_{org}$ increase and plant remains suggest wetland conditions, seems difficult to reconcile. Our preferred hypothesis is therefore to include a hiatus at 2.63 m depth.

4.2. Stratigraphy and geochemistry of Pa Kho

The stratigraphy of CP3 shows from bottom to top a fine detritus gyttja, peaty gyttja, peat and loose organic sediments (Table 1). The overall high TOC content of the sequence suggests high organic production (Fig. 3).

$\delta^{13}C_{org}$ values (-24 to -21‰) in the lowermost fine detritus and peaty gyttja (3.50-3.04 m depth; BC 170 - AD 370) indicate that the sediments contain a mix of aquatic, telmatic and terrestrial organic material (Fig. 3). Macroscopic plant remains and the presence of diatoms and phytoliths would support this. C/N ratios of 27-24, however, point to a predominantly terrestrial organic carbon source (Meyer and Teranes, 2001; Meyers, 2003) and suggest, together with elevated values for Si, K, and Ti, that run-off was important. Taken together, the proxy data indicate that Pa Kho was a shallow productive lake or a wetland with areas of open water between BC 170 and AD 370.

220 The transition from peaty gyttja to compact peat at AD 370 coincides with a distinct decrease
221 in $\delta^{13}C_{org}$ values from -23 to -28‰, an increase in BSi (phytoliths) and the occurrence of
222 terrestrial plant remains (Fig. 3). $\delta^{13}C_{org}$ values remain low between 3.04 and 2.98 m (AD
223 370-410), increase again to -24‰ between 2.98 and 2.93 m (AD 410-450), and display low,
224 but fluctuating values of -30 to - 27‰ until 2.68 m (AD 800). The overall gradual decrease in
225 the C/N ratio, which starts at 2.93 m (AD 450), may be explained by peat decomposition. This
226 process liberates soluble carbon compounds, whereas nitrogen remains relatively constant,
227 because most of its labile forms have already been consumed or transformed to inorganic
228 forms (Chimner and Ewel, 2005; Ise et al., 2008). Charcoal was observed between 2.98 and
229 2.73 m (AD 410-650), and the sample analyzed for plant remains between 2.78-2.73 m (AD
230 580-650) is composed of terrestrial-telmatic species (Fig. 3). The different proxies thus
231 suggest the development of a peatland between AD 370 and 800, but also that conditions may
232 have been variable, with a lower water table and lower effective moisture between AD 370-
233 410 and between AD 450-800, and slightly higher moisture availability between AD 410-450.

234 The marked increase in $\delta^{13}C_{org}$ values to -21‰ at 2.68 m and the shift from terrestrial-telmatic
235 to telmatic-aquatic plant assemblages at 2.66 m (Fig. 3) point to the re-establishment of a
236 wetland at Pa Kho, and thus to higher effective moisture between AD 800 and 970. The
237 subsequent hiatus suggested by the age model (CP_82_hiatus) at 2.63 m depth implies that
238 330 years are 'missing' in our record. Such a gap in a peat sequence can be caused by
239 decomposition and oxidation of the organic material under aerobic conditions. Although the
240 different processes affecting tropical peatlands are still poorly understood, a recent laboratory
241 experiment shows that drought can lead to considerable carbon loss in tropical peat samples
242 (Fenner and Freeman, 2011). Indeed, the lowest $\delta^{13}C_{org}$ values (-28‰) and the peak in BSi
243 (phytoliths) just above the hiatus, i.e. between 2.63-2.62 m (AD 1300-1340) (Fig. 3), suggest
244 an expansion of terrestrial plants onto the former wetland and generally lower effective

moisture, which persisted until 2.58 m (AD 1450). In contrast, the telmatic-aquatic plant assemblage between 2.63 and 2.60 m points to a water-saturated peat surface. This discrepancy can, however, be explained by the fact that each geochemical sample covers a one-centimeter interval, while the macrofossil sample corresponds to a three-centimeter interval and thus incorporates a mixed signal (Fig. 3). A lower and/or fluctuating water table would have led to exposure of the peat surface, and consequently to oxidation and/or biodegradation of the underlying organic material that had been accumulating between AD 970 and 1300.

The gradual increase in $\delta^{13}C_{org}$ values to -22‰ after AD 1450 (Fig. 3) and the macroscopic plant remains show that telmatic-aquatic plant material contributed to the organic carbon pool. $\delta^{13}C_{org}$ values remain constant (-24 and -25‰) between 2.51-2.02 m (AD 1510-2001), and the presence of the diatom species *Eunotia yanomami*, *Eunotia incisa*, *Eunotia intermedia*, *Eunotia monodon*, and *Gomphonema gracile* coupled with the plant macrofossil composition indicate a wetland environment.

The stepwise increase in BSi content at 2.31 m (AD 1700) and 2.07 m depth (AD 1960) may signify higher nutrient availability, and the distinct increase in major elements (Si, K, Ti) at 2.17 m depth (AD 1850) and at 2.05 m depth (AD 1970) is likely related to land-use changes around Pa Kho (Klubseang, 2011). This would suggest a significant human impact, which overprints any climate signal. The historical record around the region is not well documented, but the change seen in the Pa Kho`s sequence after AD 1700 coincides with the start of agricultural intensification in SE Asia (Lieberman and Buckley, 2012). The high C/N ratio (22), high $\delta^{13}C$ values (-22‰) and peaks of BSi, diatom and elemental data (Si, K, Ti) during the last 10 years are likely the result of the dam and intensified cultivation around the lake.

5. Discussion

The sedimentary proxies show that Pa Kho was a shallow productive lake or wetland between BC 170 and AD 370. Such an environment implies high effective moisture, likely caused by a strengthened summer monsoon. Around AD 370 the wetland transformed to a peatland with a lower water table, which suggests a decrease in effective moisture and a weakening of the summer monsoon. This transition occurred in a stepwise fashion, given that alternating intervals of lower effective moisture (AD 370-410), slightly higher effective moisture (AD 420-450) and lower effective moisture (until AD 800) are inferred (Fig. 4c). The re-establishment of a wetland between AD 800 and 970 is a sign of higher effective moisture and likely reflects increased summer monsoon precipitation. The subsequent hiatus (AD 970-1300) might have been caused by degradation of the peat surface during an interval with lower effective moisture and a weakened summer monsoon (AD 1300-1450) (Fig. 4c). The increase in aquatic plant remains, the appearance of diatoms and the isotope proxies show again a wetland environment starting around AD 1450. This marks a return to higher effective moisture and a moderately strengthened summer monsoon. The geochemical proxies established for CP3 can be compared with the multi-sediment and multi-proxy records of Lake Kumphawapi, which is located 15 km to the northeast. These showed the re-establishment of a shallow lake around AD 150-350 and suggested higher effective moisture and a strengthened summer monsoon (Chawchai et al., 2013; Wohlfarth et al., 2012), similar to our interpretation of the Pa Kho record. However, a detailed interpretation of the paleoenvironment in Kumphawapi after AD 350 is limited due to chronological uncertainties.

Given the lack of paleo-precipitation records from tropical lakes and wetland in Southeast Asia, it is important to examine whether the environmental signals stored in Pa Kho´s sequence are a reflection of summer monsoon variability. To infer spatial patterns of

hydroclimatic variability, we compare the Pa Kho data set to selected high-resolution paleoclimatic records established for the Asian monsoon region. The stronger/weaker summer monsoon intervals presented in Figures 4 a-f follow the interpretation of the respective authors and present a fairly coherent picture of Asian summer monsoon variability. The terrestrial plant leaf wax (δD_{wax}) record established from marine sediments from the Makassar Strait, Southwest Sulawesi (Tierney et al., 2010) is the only high-resolution record extending as far back as Pa Kho, while the Wanxiang Cave $\delta^{18}O$ data set commences around AD 200 (Zhang et al. 2008). All other high-resolution records only cover the last 1400 years (central India composite record) (Berkelhammer et al. 2010; Sinha et al. 2011a, 2011b, 2007); the last 1000 years (Dongdao Island) (Yan et al., 2011) or the past 700-800 years (MADA data set; Dayu Cave) (Buckley et al., 2007, 2010, 2014; Cook et al., 2010; Tan et al., 2009) (Fig. 4a-f).

Higher effective moisture (BC 170 – AD 370), followed by a stepwise decline (AD 370-450) and lower moisture availability (AD 450-800) as reconstructed for Pa Kho is comparable with the $\delta^{18}O$ record from Wanxiang Cave in central China (Fig. 4a, c). This record suggests that the summer monsoon was moderately strong between AD 190-530, gradually declined after AD 530 and was markedly weaker between AD 860-940 (Zhang et al., 2008) (Fig. 4a, c). The offset of 60 to 140 years between the two data sets at the beginning and end of the weaker summer monsoon period, respectively, may stem from chronological uncertainties. Upwelling indicators *(Globigerina bulloides)* in sediments from the northwestern Arabian Sea also show a weakening of the summer monsoon starting around AD 450 (Anderson et al., 2010, 2002), and the composite speleothem $\delta^{18}O$ records from Indian caves give evidence for decadal intervals of a distinctly weaker summer monsoon between AD 650-900 (Berkelhammer et al., 2010; Sinha et al., 2011a, 2007) (Fig. 4b). These time intervals of a stronger/weaker Asian summer monsoon, however, differ from to the δD_{wax} record from the Makassar Strait (Fig. 4a-

317 c, f), which suggests a weaker Asian monsoon until around AD 450 and subsequently a
318 stronger monsoon until about AD 1000 (Tierney et al., 2010) (Fig. 4f).

319 Berkelhammer et al. (2010), Sinha et al. (2011a, 2007) and Zhang et al. (2008) infer a
320 strengthening of the summer monsoon between AD 950-1300 from speleothem $\delta^{18}O$ records
321 (Fig. 4a, b). These findings are comparable within error margins to our data set, which
322 suggests higher effective moisture starting around AD 800 (Fig. 4c), but they differ from
323 lower precipitation inferred over Dongdao Island in the South China Sea between AD 1000-
324 1400 (Yan et al., 2011) (Fig. 4d). δD_{wax} values from the Makassar Strait also imply a weaker
325 summer monsoon throughout the period AD 1000-1350 (Tierney et al., 2010) (Fig. 4f).

326 The Pa Kho data set gives evidence for distinctly lower effective moisture between AD 1300
327 and 1450. This coincides, within error margins, with the start of a weaker summer monsoon
328 phase recorded in Wanxiang Cave (Zhang et al., 2008) (Fig. 4a), and also compares to the
329 intervals of lower precipitation (AD 1249-1325; 1390-1420) inferred from speleothem $\delta^{18}O$
330 values in Dayu Cave (Tan et al., 2009). Decreased upwelling in the Arabian Sea (AD 1350-
331 1550) is also interpreted as a weakening of the Asian summer monsoon (Anderson et al.,
332 2010, 2002). Distinct decadal-long droughts are recognized in the $\delta^{18}O$ records of Indian cave
333 speleothems between AD 1300-1450 (Berkelhammer et al., 2010; Sinha et al., 2011a, 2011b,
334 2007), in the MADA tree-ring data set (AD 1340-1370; 1400-1425) and in the sediment
335 proxies from the West Baray reservoir at Angkor, Cambodia (AD 1300-1400) (Buckley et al.,
336 2007, 2010; Cook et al., 2010; Day et al., 2012) (Fig. 4b, e). The Dongdao Island (Yan et al.,
337 2011, 2011) and Makassar Strait (Tierney et al. 2010) records on the other hand imply a shift
338 towards a strengthened summer monsoon around AD 1350-1400 (Fig. 4d, f).

339 The inferred moisture history for Pa Kho since AD 1450 (Fig. 4c) compares well to the
340 moderately intense summer monsoon reconstructed from Indian cave speleothems

(Berkelhammer et al., 2010; Sinha et al., 2011a, 2011b, 2007) and Arabian Sea proxies (Anderson et al., 2010, 2002), but seems to diverge from the hydroclimatic scenario established for Wanxiang Cave (Zhang et al. 2008). A correspondence can also be found between the Pa Kho record and climate inferences for Dongdao Island and southwest Sulawesi, where higher precipitation has been reconstructed since AD 1400 (Fig. 4d, f) (Tierney et al., 2010; Yan et al., 2011). It is interesting, however, to note that the interpretation of the speleothem $\delta^{18}O$ records from Wanxiang Cave (Zhang et al., 2008) and neighboring Dayu Cave (Tan et al., 2009) do not correspond to each other. For Wanxiang Cave, a generally weaker summer monsoon is reconstructed throughout the time interval AD 1350-1850 (Zhang et al., 2008), whereas the Dayu Cave record suggests a weaker summer monsoon around AD 1300-1400, an increase in summer monsoon intensity around AD 1500, intervals of higher monsoon precipitation between AD 1535-1685, AD 1755-1835 and AD 1920-1970, and lower precipitation between AD 1890-1915 (Tan et al., 2009). When Li et al. (2014) compared speleothem $\delta^{18}O$ records from a region spanning from 60° to 125°E and from 10° to 40° N, they observed similar and divergent precipitation patterns in close-by speleothem records from China. This would suggest that monsoon precipitation on decadal and centennial time scales varied regionally and that the response to climate change between and within each monsoon sub-system is complicated. The obvious differences between the two speleothem data sets starting around AD 1500 would imply that speleothem $\delta^{18}O$ values do not provide a straightforward measure for large-scale regional summer monsoon intensity, but that they also record sub-regional precipitation signals, or that a number of other factors are involved in creating the $\delta^{18}O$ signal (Li et al., 2014).

Sinha et al. (2011) note a distinct shift in precipitation patterns around AD 1650-1700, when $\delta^{18}O$ values from caves in northern and central India start to diverge. Records from central India suggest a shift from drier to wetter conditions, while the northern Indian caves indicate a

366 shift from wetter to drier conditions. This shift in precipitation patterns has been interpreted as
367 reflecting active and break phases of the Indian summer monsoon (Sinha et al., 2011a). The
368 decadal droughts during the 17th and 18th centuries registered in Indian cave speleothems
369 (Berkelhammer et al., 2010; Sinha et al., 2011a, 2011b, 2007) and in the MADA data set
370 (Buckley et al., 2007, 2010, 2014; Cook et al., 2010; D'Arrigo et al., 2011; Sano et al., 2009)
371 are not recognized in the Pa Kho proxies (Fig. 4 b-e). This is likely due to the lower temporal
372 resolution as compared to the tree-ring and speleothem records, but it could also be that
373 human impact overprinted any climatic signals.

374 The opposing hydroclimatic patterns seen between Wanxiang Cave and Pa Kho in the north
375 and southwest Sulawesi in the south can be explained by their location relative to the
376 migration of the ITCZ (Sinha et al., 2011b; Tierney et al., 2010), and by interactions between
377 the Asian-Australian monsoon systems. A strengthened Asian summer monsoon between BC
378 170 - AD 500 and between AD 900-1300, in combination with a weak Australian monsoon,
379 would have led to a shift of the tropical rain belt northward of Indonesia, leading to drought in
380 equatorial regions. The opposite would have been the case between AD 500-900 and between
381 AD 1300-1450, when the Asian summer monsoon weakened and the mean position of the
382 tropical rain belt shifted over Indonesia. This hydroclimatic scenario seems to have changed
383 after AD 1450, when the two neighboring Chinese cave records show opposing dry/wet
384 patterns, the northeast Indian cave speleothems a shift to dry conditions and the central Indian
385 caves a shift to wetter condition, while Pa Kho shows patterns similar to those on Dongdao
386 Island and in Southwest Sulawesi (Fig. 4a-f). Independent of the differences between
387 Wanxiang and Dayu Caves, which could stem from local factors, we may assume that the
388 effect of a moderately strengthened summer monsoon was only registered as far north as 20°
389 N, while rainfall was strong over the equatorial region. We thus hypothesize that the mean
390 summer position of the ITCZ over land did not reach as far north as during the strengthened

summer monsoon intervals before AD 1450 and that it was located approximately where it is today (Fig. 5). Similar conclusions have been drawn based on a record from the central equatorial Pacific (Sachs et al., 2009).

Decadal drought intervals during the past 700-800 years seen in the in the MADA tree ring data series and in Dayu Cave speleothems have been linked to ENSO variability (Cook et al. 2010; Tan et al. 2009). However, the moisture history derived from Wanxiang Cave has been associated with solar influence and climate variability in the North Atlantic region (Zhang et al. 2008). Decadal drought observed in the Indian speleothems, on the other hand, have been linked to Indian Ocean variability (Sinha et al. 2011). The centennial-scale shifts in hydroclimatic conditions reconstructed for Pa Kho support shifts in the mean position of the ITCZ as these produced associated changes in summer monsoon precipitation. IOD and ENSO events also may have had important influences on monsoon rainfall on decadal time scales, but these are not clearly registered in our centennial- scale record.

A more precise reconstruction of the temporal and spatial variability of past monsoon precipitation patterns and their underlying causes would require several additional high-resolution hydroclimatic records from the Asian monsoon region. Only a dense network of well-dated, multi-proxy data sets can help to reduce the current uncertainties in interpretation and provide a valid base for evaluating the inherent leads and lags of different proxies used to infer hydroclimatic conditions.

Conclusions

The new hydroclimatic reconstruction based on the high-resolution data set established for Lake Pa Kho in northeast Thailand adds important information in data coverage between China and Indonesia during the last two millennia. The multi-proxy study of the Pa Kho

sequence reveals time intervals when the summer monsoon was strengthened (BC 170-AD 370, AD 800 – 960, and since AD 1450) and time intervals of drought (AD 370–800 and AD 1300-1450). Within error margins the effective moisture variability (BC 170 – AD 1450) reconstructed for Pa Kho is comparable to hydroclimatic patterns derived from speleothem proxies in China and India. The drought intervals expressed in these records compare to intervals of stronger monsoonal rainfall in equatorial regions, as shown by the record from the Makassar Strait in Indonesia. This hydroclimatic pattern seems to have changed sometime between AD 1450-1600, when the inferred moisture history for Pa Kho became more similar to that reconstructed for the South China Sea and the Indonesian region. This would suggest that the mean position of the ITCZ over land generally did not reach as far north as it did prior to AD 1450.

Acknowledgments

We thank Rienk H. Smittenberg and Kweku Afrifa Yamoah for discussions about the geochemistry and Francesco Muschitiello for discussions about age models. Kevin J. Anchukaitis and Karina Schollaen provided the SE Asian tree ring data sets and Hong Yan those for Cattle Pond. Jan Risberg, and Shyhrete Shala helped with the diatom and phytolith analyses and Wichuratree Klubseang provided the digital file, which was used to draw the map in Figure 1B. Heike Sigmund and the Stable Isotope Laboratory at the Department of Geological Sciences, Stockholm University are acknowledged for analyzing total and CN isotopes. Research in Thailand was financed through Swedish Research Council (VR) research grants 621-2008-2855 and 348-2008-6071. S. Chawchai acknowledges financial support from the Royal Thai Government Scholarship under the DPST project.

Figure text

Figure 1. (A) Location of the study area in northeast Thailand. (B) Topography around Pa Kho and the location of coring point CP3. The coordinate system is based on the UTM Grid system (WGS 1984 zone 48; asl = above sea level). (C) Mean monthly rainfall and temperature (1962-2011) for Udon Thani, which is situated 36 km NW of Pa Kho. Map (A) was generated using the generic mapping tools-GMT (http://gmt.soest.hawaii.edu/), and map (B) was redrawn based on aerial photographs before and after 1994 using the data set in Klubseang (2011).

Figure 2. (A) Lithostratigraphy for CP3, (B) age model CP3_82 and (C) age model CP3_82_hiatus. The blue shapes show the calibrated ^{14}C dates with two standard deviations, the grey shading indicates the likely age model and the dotted lines show the 95% confidence ranges of the age model. See Table 1 for a detailed description of the sequence and Table 2 for the ^{14}C dates.

Figure 3. Lithostratigraphy, geochemistry, and selected elemental data for CP3. The samples analyzed for diatoms, phytoliths, charcoal, and plant macrofossil composition are discontinuous (see text for further explanations). Light gray bars represent higher effective moisture, and the dark gray bars represent lower effective moisture.

Figure 4. Selected high-resolution records for the Asian monsoon region for the past 2000 years: (a) $\delta^{18}O$ data of Wanxiang Cave speleothems (Zhang et al., 2008); (b) Composite $\delta^{18}O$ time series for central India based on speleothems from Dandak, Jhumar, and Wah Shikar Caves (Berkelhammer et al. 2010; Sinha et al. 2011a, 2011b, 2007); (c) $\delta^{13}C_{org}$ data from Lake Pa Kho (this study); (d) grain size variations in sediment core DY6-MGS of Cattle Pond, Dongdao Island (Yan et.al, 2011); (e) Palmer Drought Severity Index (PDSI) derived from the Monsoon Asia Drought Atlas (MADA) for the region between 10-20°N and 95-

115°E (Buckley et al., 2007, 2010, 2014; Cook et al., 2010; D'Arrigo et al., 2011; Sano et al., 2009); (f) δD_{wax} from marine cores 31MC and 34GGC from southwest Sulawesi (Tierney et al., 2010). The vertical light gray bars represent higher effective moisture/a strengthened summer monsoon, and the dark gray bars represent lower effective moisture/a weakened summer monsoon. Note that the timing of the shifts in moisture history of the individual records follows that cited by the respective author/s. See Figure 5 for the location of the different records.

Figure 5. Location of selected high-resolution Asian monsoon paleo-records for the last 2000 years. The mean position of the winter and summer Intertropical Convergence Zone (ITCZ) is according to Wang (2009). The July-August wind directions and wind speeds follow Wang et al. (2003). Long arrows indicate high wind speed and short arrows lower wind speed.

Table text

Table 1. Lithostratigraphic description, plant macrofossil composition of selected samples and inferred depositional environment for CP3.

Table 2 ^{14}C dates for CP3. Core depth (in m) is given below the water surface. See Figure 1 for the location of the coring point. The stratigraphic units relate to those shown in Table 1.

References

Anderson, D.M., Baulcomb, C.K., Duvivier, A.K., Gupta, A.K., 2010. Indian summer monsoon during the last two millennia. Journal of Quaternary Science 25, 911–917. doi:10.1002/jqs.1369

Anderson, D.M., Overpeck, J.T., Gupta, A.K., 2002. Increase in the Asian Southwest Monsoon During the Past Four Centuries. Science 297, 596–599. doi:10.1126/science.1072881

489 Berkelhammer, M., Sinha, A., Mudelsee, M., Cheng, H., Edwards, R.L., Cannariato, K.,
490 2010. Persistent multidecadal power of the Indian Summer Monsoon. Earth and
491 Planetary Science Letters 290, 166–172. doi:10.1016/j.epsl.2009.12.017
492 Blaauw, M., Christen, J., 2011. Flexible paleoclimate age-depth models using an
493 autoregressive gamma process. Bayesian Analysis 6, 457–474.
494 Bridhikitti, A., 2013. Connections of ENSO/IOD and aerosols with Thai rainfall anomalies
495 and associated implications for local rainfall forecasts. International Journal of
496 Climatology 33, 2836–2845. doi:10.1002/joc.3630
497 Buckley, B., Palakit, K., Duangsathaporn, K., Sanguantham, P., Prasomsin, P., 2007. Decadal
498 scale droughts over northwestern Thailand over the past 448 years: links to the tropical
499 Pacific and Indian Ocean sectors. Climate Dynamics 29, 63–71. doi:10.1007/s00382-
500 007-0225-1
501 Buckley, B.M., Anchukaitis, K.J., Penny, D., Fletcher, R., Cook, E.R., Sano, M., Nam, L.C.,
502 Wichienkeeo, A., Minh, T.T., Hong, T.M., 2010. Climate as a contributing factor in
503 the demise of Angkor, Cambodia. Proceedings of the National Academy of Sciences
504 107, 6748–6752. doi:10.1073/pnas.0910827107
505 Buckley, B.M., Fletcher, R., Wang, S.-Y.S., Zottoli, B., Pottier, C., 2014. Monsoon extremes
506 and society over the past millennium on mainland Southeast Asia. Quaternary Science
507 Reviews 95, 1–19. doi:10.1016/j.quascirev.2014.04.022
508 Chabangborn, A., 2014. Asian monsoon over mainland Southeast Asia in the past 25000
509 years. PhD Thesis, Stockholm University, Stockholm, Sweden, 65pp.
510 Chawchai, S., Chabangborn, A., Kylander, M., Löwemark, L., Mörth, C.-M., Blaauw, M.,
511 Klubseang, W., Reimer, P.J., Fritz, S.C., Wohlfarth, B., 2013. Lake Kumphawapi – an
512 archive of Holocene palaeoenvironmental and palaeoclimatic changes in northeast
513 Thailand. Quaternary Science Reviews 68, 59–75.
514 doi:10.1016/j.quascirev.2013.01.030
515 Chimner, R.A., Ewel, K.C., 2005. A Tropical Freshwater Wetland: II. Production,
516 Decomposition, and Peat Formation. Wetlands Ecology and Management 13, 671–
517 684. doi:10.1007/s11273-005-0965-9
518 Cobb, K.M., Charles, C.D., Cheng, H., Edwards, R.L., 2003. El Niño/Southern Oscillation
519 and tropical Pacific climate during the last millennium. Nature 424, 271–276.
520 doi:10.1038/nature01779
521 Cook, E.R., Anchukaitis, K.J., Buckley, B.M., D'Arrigo, R.D., Jacoby, G.C., Wright, W.E.,
522 2010. Asian Monsoon Failure and Megadrought During the Last Millennium. Science
523 328, 486–489. doi:10.1126/science.1185188
524 D'Arrigo, R., Palmer, J., Ummenhofer, C.C., Kyaw, N.N., Krusic, P., 2011. Three centuries
525 of Myanmar monsoon climate variability inferred from teak tree rings. Geophysical
526 Research Letters 38, L24705. doi:10.1029/2011GL049927
527 Day, M.B., Hodell, D.A., Brenner, M., Chapman, H.J., Curtis, J.H., Kenney, W.F., Kolata,
528 A.L., Peterson, L.C., 2012. Paleoenvironmental History of the West Baray, Angkor
529 (Cambodia). Proceedings of the National Academy of Sciences 109, 1046–1051.
530 doi:10.1073/pnas.1111282109
531 El Tabakh, M., Utha-Aroon, C., Warren, J.K., Schreiber, B.C., 2003. Origin of dolomites in
532 the Cretaceous Maha Sarakham evaporites of the Khorat Plateau, northeast Thailand.
533 Sedimentary Geology 157, 235–252. doi:10.1016/S0037-0738(02)00235-X
534 Fenner, N., Freeman, C., 2011. Drought-induced carbon loss in peatlands. Nature Geoscience
535 4, 895–900. doi:10.1038/ngeo1323
536 Hsu, H.-H., Zhou, T., Matsumoto, J., 2014. East Asian, Indochina and Western North Pacific
537 Summer Monsoon - An update. Asia-Pacific Journal of Atmospheric Sciences 50, 45–
538 68. doi:10.1007/s13143-014-0027-4

539 Ise, T., Dunn, A.L., Wofsy, S.C., Moorcroft, P.R., 2008. High sensitivity of peat
540 decomposition to climate change through water-table feedback. Nature Geoscience 1,
541 763–766. doi:10.1038/ngeo331
542 Klubseang, W., 2011. Paleogeography and paleoenvironment of Nong Han Kumphawapi,
543 Changwat Udon Thani. MSc thesis Chulalongkorn University,Bangkok 1–110.
544 Kuhry, P., Vitt, D.H., 1996. Fossil Carbon/Nitrogen Ratios as a Measure of Peat
545 Decomposition. Ecology 77, 271–275. doi:10.2307/2265676
546 Kylander, M.E., Ampel, L., Wohlfarth, B., Veres, D., 2011. High-resolution X-ray
547 fluorescence core scanning analysis of Les Echets (France) sedimentary sequence:
548 new insights from chemical proxies. Journal of Quaternary Science 26, 109–117.
549 doi:10.1002/jqs.1438
550 Li, Y., Wang, N., Zhou, X., Zhang, C., Wang, Y., 2014. Synchronous or asynchronous
551 Holocene Indian and East Asian summer monsoon evolution: A synthesis on Holocene
552 Asian summer monsoon simulations, records and modern monsoon indices. Global
553 and Planetary Change 116, 30–40. doi:10.1016/j.gloplacha.2014.02.005
554 Lieberman, V., Buckley, B., 2012. The Impact of Climate on Southeast Asia, circa 950–1820:
555 New Findings. Modern Asian Studies FirstView, 1–48.
556 Limsakul, A., Paengkaew, W., Kummueang, A., Limjirakan, S., Suttamanuswong, B., 2011.
557 PDSI-based variations of droughts and wet spells in Thailand: 1951-2005.
558 Environment Asia 4, 12–20.
559 Mann, M.E., Zhang, Z., Rutherford, S., Bradley, R.S., Hughes, M.K., Shindell, D., Ammann,
560 C., Faluvegi, G., Ni, F., 2009. Global Signatures and Dynamical Origins of the Little
561 Ice Age and Medieval Climate Anomaly. Science 326, 1256–1260.
562 doi:10.1126/science.1177303
563 Meyer, P.A., Teranes, J.., 2001. Sediment organic matter. In: Last, W.M., Smol, J.P. (EDs),
564 Tracking Environmental Change Using Lake Sediments: Physical and Geochemical
565 Methods. Dordrecht.
566 Meyers, P.A., 2003. Applications of organic geochemistry to paleolimnological
567 reconstructions: a summary of examples from the Laurentian Great Lakes. Organic
568 Geochemistry 34, 261–289. doi:10.1016/S0146-6380(02)00168-7
569 Newton, A., Thunell, R., Stott, L., 2006. Climate and hydrographic variability in the Indo-
570 Pacific Warm Pool during the last millennium. Geophysical Research Letters 33,
571 L19710. doi:10.1029/2006GL027234
572 Oppo, D.W., Rosenthal, Y., Linsley, B.K., 2009. 2,000-year-long temperature and hydrology
573 reconstructions from the Indo-Pacific warm pool. Nature 460, 1113–1116.
574 doi:10.1038/nature08233
575 Pages 2K, Consortium, 2013. Continental-scale temperature variability during the past two
576 millennia. Nature Geoscience 6, 339–346. doi:10.1038/ngeo1797
577 Penny, D., 1998. Late Quaternary Palaeoenvironments in the Sakon Nakhon Basin,North-east
578 Thailand.PhD Thesis, Monash University, Victoria/Australia, 260pp.
579 Penny, D., 2001. A 40,000 year palynological record from north-east Thailand; implications
580 for biogeography and palaeo-environmental reconstruction. Palaeogeography,
581 Palaeoclimatology, Palaeoecology 171, 97–128. doi:10.1016/S0031-0182(01)00242-5
582 Prasad, S., Anoop, A., Riedel, N., Sarkar, S., Menzel, P., Basavaiah, N., Krishnan, R., Fuller,
583 D., Plessen, B., Gaye, B., Röhl, U., Wilkes, H., Sachse, D., Sawant, R., Wiesner,
584 M.G., Stebich, M., 2014. Prolonged monsoon droughts and links to Indo-Pacific warm
585 pool: A Holocene record from Lonar Lake, central India. Earth and Planetary Science
586 Letters 391, 171–182. doi:10.1016/j.epsl.2014.01.043

587 Sachs, J.P., Sachse, D., Smittenberg, R.H., Zhang, Z., Battisti, D.S., Golubic, S., 2009.
588 Southward movement of the Pacific intertropical convergence zone AD 1400–1850.
589 Nature Geoscience 2, 519–525. doi:10.1038/ngeo554
590 Sano, M., Buckley, B.M., Sweda, T., 2009. Tree-ring based hydroclimate reconstruction over
591 northern Vietnam from Fokienia hodginsii: eighteenth century mega-drought and
592 tropical Pacific influence. Climate Dynamics 33, 331–340. doi:10.1007/s00382-008-
593 0454-y
594 Singhrattna, N., Rajagopalan, B., Kumar, K.K., Clark, M., 2005. Interannual and Interdecadal
595 Variability of Thailand Summer Monsoon Season. Journal of Climate 18, 1697–1708.
596 doi:10.1175/JCLI3364.1
597 Sinha, A., Berkelhammer, M., Stott, L., Mudelsee, M., Cheng, H., Biswas, J., 2011a. The
598 leading mode of Indian Summer Monsoon precipitation variability during the last
599 millennium. Geophysical Research Letters 38. doi:10.1029/2011GL047713
600 Sinha, A., Cannariato, K.G., Stott, L.D., Cheng, H., Edwards, R.L., Yadava, M.G., Ramesh,
601 R., Singh, I.B., 2007. A 900-year (600 to 1500 A.D.) record of the Indian summer
602 monsoon precipitation from the core monsoon zone of India. Geophysical Research
603 Letters 34, L16707. doi:10.1029/2007GL030431
604 Sinha, A., Stott, L., Berkelhammer, M., Cheng, H., Edwards, R.L., Buckley, B., Aldenderfer,
605 M., Mudelsee, M., 2011b. A global context for megadroughts in monsoon Asia during
606 the past millennium. Quaternary Science Reviews 30, 47–62.
607 doi:10.1016/j.quascirev.2010.10.005
608 Tan, L., Cai, Y., Cheng, H., An, Z., Edwards, R.L., 2009. Summer monsoon precipitation
609 variations in central China over the past 750 years derived from a high-resolution
610 absolute-dated stalagmite. Palaeogeography, Palaeoclimatology, Palaeoecology 280,
611 432–439. doi:10.1016/j.palaeo.2009.06.030
612 Tierney, J.E., Oppo, D.W., Rosenthal, Y., Russell, J.M., Linsley, B.K., 2010. Coordinated
613 hydrological regimes in the Indo-Pacific region during the past two millennia.
614 Paleoceanography 25, PA1102. doi:10.1029/2009PA001871
615 Ummenhofer, C.C., D'Arrigo, R.D., Anchukaitis, K.J., Buckley, B.M., Cook, E.R., 2013.
616 Links between Indo-Pacific climate variability and drought in the Monsoon Asia
617 Drought Atlas. Climate Dynamics 40, 1319–1334. doi:10.1007/s00382-012-1458-1
618 Wang, B., Clemens, S.C., Liu, P., 2003. Contrasting the Indian and East Asian monsoons:
619 implications on geologic timescales. Marine Geology 201, 5–21. doi:10.1016/S0025-
620 3227(03)00196-8
621 Wang, P., 2009. Global monsoon in a geological perspective. Chinese Science Bulletin 54,
622 1113–1136. doi:10.1007/s11434-009-0169-4
623 Wang, P., Clemens, S., Beaufort, L., Braconnot, P., Ganssen, G., Jian, Z., Kershaw, P.,
624 Sarnthein, M., 2005. Evolution and variability of the Asian monsoon system: state of
625 the art and outstanding issues. Quaternary Science Reviews 24, 595–629.
626 doi:10.1016/j.quascirev.2004.10.002
627 Wang, Y., Cheng, H., Edwards, R.L., He, Y., Kong, X., An, Z., Wu, J., Kelly, M.J., Dykoski,
628 C.A., Li, X., 2005. The Holocene Asian Monsoon: Links to Solar Changes and North
629 Atlantic Climate. Science 308, 854–857. doi:10.1126/science.1106296
630 Wannakomol, A., 2005. Soil and groundwater salinization problems in the Khorat Plateau,
631 NE Thailand integrated study of remote sensing, geophysical and field data. Freie
632 Universität Berlin, Berlin.
633 Wohlfarth, B., Klubseang, W., Inthongkaew, S., Fritz, S.C., Blaauw, M., Reimer, P.J.,
634 Chabangborn, A., Löwemark, L., Chawchai, S., 2012. Holocene environmental
635 changes in northeast Thailand as reconstructed from a tropical wetland. Global and
636 Planetary Change 92–93, 148–161. doi:10.1016/j.gloplacha.2012.05.008

637 Yan, H., Sun, L., Oppo, D.W., Wang, Y., Liu, Z., Xie, Z., Liu, X., Cheng, W., 2011. South
638 China Sea hydrological changes and Pacific Walker Circulation variations over the
639 last millennium. Nature Communications 2, 293. doi:10.1038/ncomms1297
640 Yancheva, G., Nowaczyk, N.R., Mingram, J., Dulski, P., Schettler, G., Negendank, J.F.W.,
641 Liu, J., Sigman, D.M., Peterson, L.C., Haug, G.H., 2007. Influence of the intertropical
642 convergence zone on the East Asian monsoon. Nature 445, 74–77.
643 doi:10.1038/nature05431
644 Zhang, P., Cheng, H., Edwards, R.L., Chen, F., Wang, Y., Yang, X., Liu, J., Tan, M., Wang,
645 X., Liu, J., An, C., Dai, Z., Zhou, J., Zhang, D., Jia, J., Jin, L., Johnson, K.R., 2008. A
646 Test of Climate, Sun, and Culture Relationships from an 1810-Year Chinese Cave
647 Record. Science 322, 940–942. doi:10.1126/science.1163965
648

Table 1 Lithostratigraphic description, plant macrofossil composition of selected samples and inferred depositional environment for CP3.

Depth (m) below water surface	Lithostratigraphic description	Units	Composition of plant macro remains	Inferred depositional environment
2.00-2.02	Loose orgainic sediment	1	Depth 2.20-2.23 m:	Aquatic
2.02-2.04	Dark brown peat, compact		Occasional plant remains	
2.04-2.22	Dark brown fibrous peat			
2.22-2.73	Dark brown soft fibrous peat; loose soft peat between 2.33-2.68 m	2	Depth 2.54-2.57 m: Large pieces of aquatic plant remains (e.g. *Potamogeton*); Cyperaceae spp., *Typha* and Poaceae seeds.	Aquatic
			Depth 2.60-2.63 m: Woody fragments, plant remains, Cyperaceae spp., *Utricularia*, *Najas* and *Nymphoides indicum* seeds; macroscopic charcoal.	Aquatic– telmatic
			Depth 2.63-2.66 m: Plant remains; Cyperaceae spp., *Nympoides indicum*, *Typha* and Poaceae seeds; macroscopic charcoal.	Aquatic– telmatic
			Depth 2.66-2.69 m: Relatively high amount of plant remains, woody remains and Cyperaceae spp. and *Nymphoides indicum* seeds.	Telmatic-terrestrial
2.73-3.04	Dark brown compact peat	3	Depth 2.73-2.78 m: Plant remains and Poaceae seeds.	Telmatic-terrestrial
			Depth 2.98-3.04 m: Coarse organic material, e.g. large wood remains; charred plant remains and Cyperaceae spp. seeds.	Terrestrial
3.04-3.34	Dark brown peaty gyttja/ coarse detritus gyttja with some fibrous peat horizons	4	Depth 3.32-3.36 m: Fine light roots and other plant remains; *Nymphaea*, Cyperaceae spp., *Typha*, *Scirpus*, *Utricularia* and Poaceae seeds.	Aquatic– telmatic
3.34-3.36	Transition zone between unit 5 and 4			
3.36-3.50	Dark brown fine detritus gyttja with some peaty horizons	5	Depth 3.44-3.48 m: Occasional plant remains	Aquatic

Table 2 ^{14}C dates for CP3. Core depth (in m) is given below the water surface. See Figure 1 for the location of the coring point. The stratigraphic units relate to those shown in Table 1. * = undetermined

Lab ID	Core depth (m)	^{14}C date BP ±1 σ	Dated material	Unit
UBA-23310	2.10-2.13	188±24	*Scirpus*, *Nymphaea*, Cyperaceae seeds; charcoal, insects, wood piece	1
UBA-18074	2.20-2.23	299±23	Seeds*, charcoal, insects	1
UBA-14635	2.54-2.57	410±38	Seeds*, charcoal, wood	2
UBA-18075	2.57-2.60	434±23	Seeds*, charcoal, wood	2
UBA-23756	2.60-2.63	638±31	*Nymphaea* seeds, charcoal, charred plant remains, wood, bark, insects	2
UBA-19839	2.60-2.63	687±23	Seeds*	2
UBA-14636	2.63-2.66	1153±26	Seeds*, charcoal, wood	2
UBA-12777	2.70-2.73	1388±22	Plant remains*	2
UBA-19840	2.70-2.73	1312±25	Seeds*, insects, leaf fragments*	2
UBA-23311	2.73-2.78	1459±28	*Nymphaea*, Cyperaceae seeds; charcoal, insects, leaf fragments*	3
UBA-23312	2.78-2.83	1777±34	*Nymphaea*, Cyperaceae seeds; charcoal, wood, leaf fragment*	3
UBA-23313	2.83-2.88	1587±25	*Nymphaea*, *Scirpus*, Cyperaceae seeds; charcoal, insects, leaf fragments*	3
UBA-18076	2.88-2.93	1602±24	Seeds*, charcoal, insects	3
UBA-14637	2.93-2.98	1611±21	Charcoal	3
UBA-19837	3.10-3.13	1625±25	Seeds*, insects, leaf fragments*	4
UBA-18077	3.30-3.33	1822±28	Seeds*, insects, leaf fragments*	4
UBA-14639	3.40-3.44	1873±32	Small wood fragments	5
UBA-19841	3.40-3.44	2465±29	Seeds*, leaf fragments, charcoal	5
UBA-16756	3.44-3.48	2083±25	Seeds*, charcoal, wood, leaf fragments*	5
UBA-23283	3.48-3.52	2050±28	Small wood fragments, plant remains*	5

*Figure 1

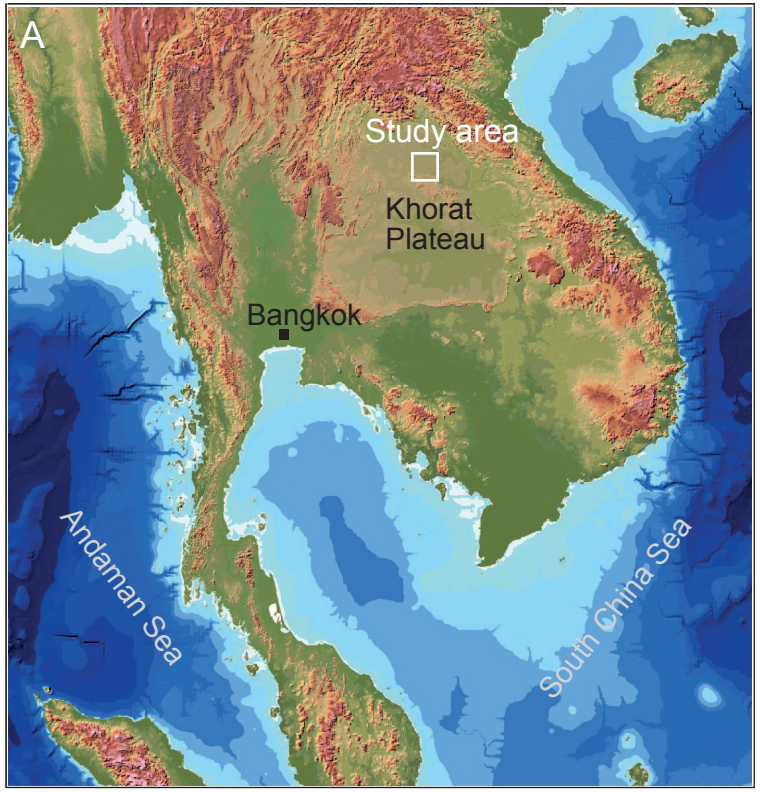
A
Study area
Khorat
Plateau
Bangkok
Andaman Sea
South China Sea

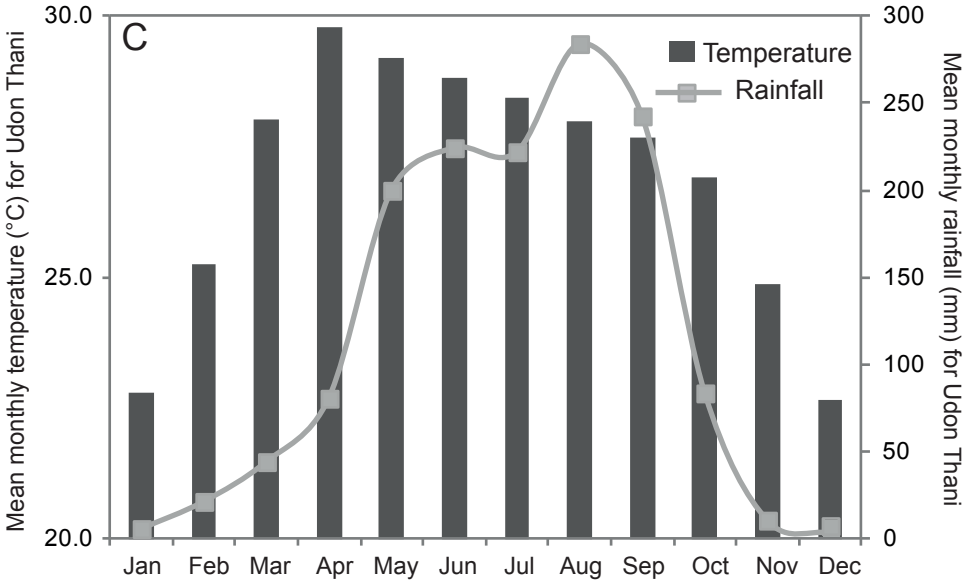
C
Temperature
Rainfall
Mean monthly temperature (°C) for Udon Thani
Mean monthly rainfall (mm) for Udon Thani
30.0
25.0
20.0
300
250
200
150
100
50
0
Jan
Feb
Mar
Apr
May
Jun
Jul
Aug
Sep
Oct
Nov
Dec

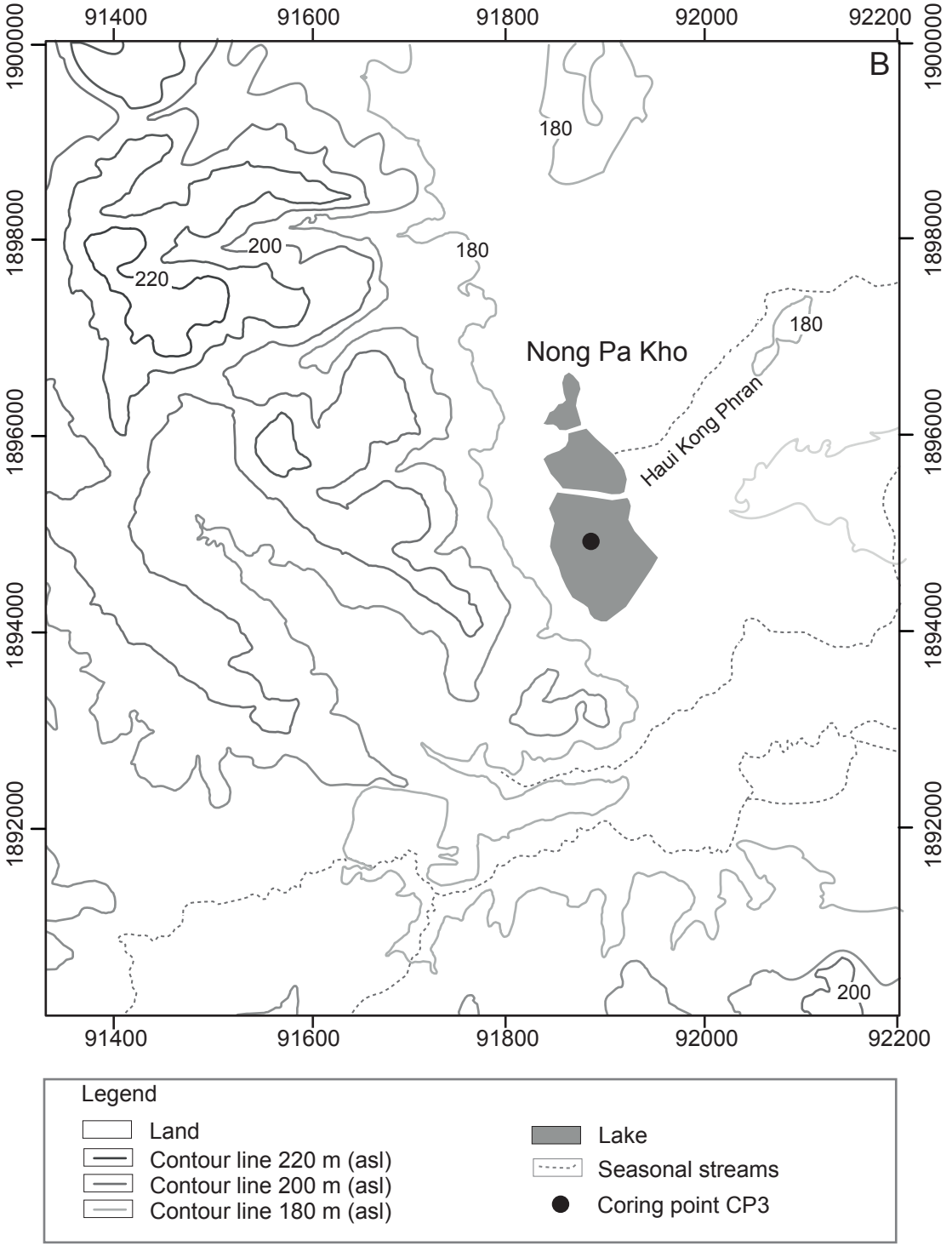
B
91400
91600
91800
92000
92200
1900000
1898000
1896000
1894000
1892000
180
200
220
Nong Pa Kho
Haui Kong Phran
Legend
Land
Contour line 220 m (asl)
Contour line 200 m (asl)
Contour line 180 m (asl)
Lake
Seasonal streams
Coring point CP3

Figure2
Figure 2

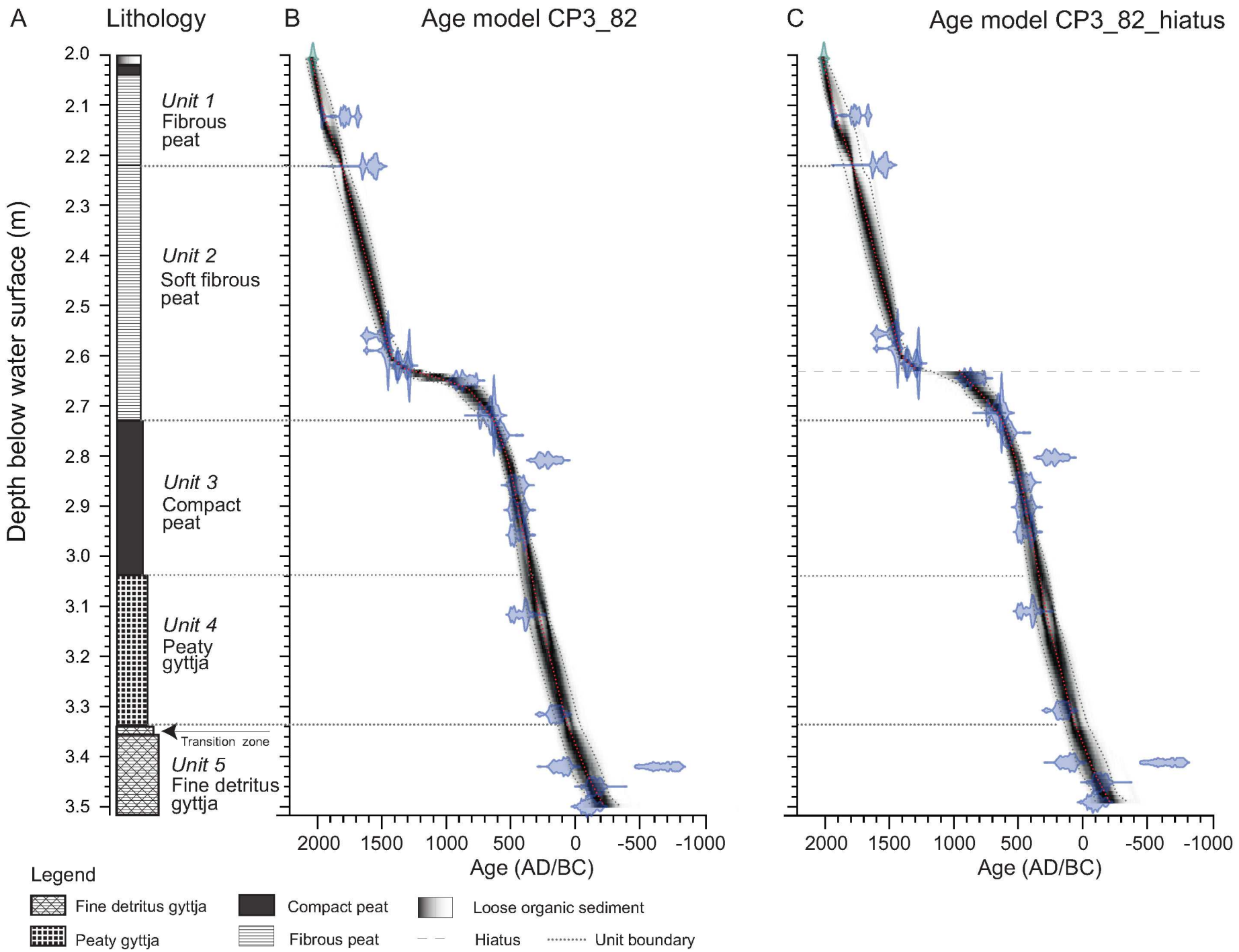

Figure 3

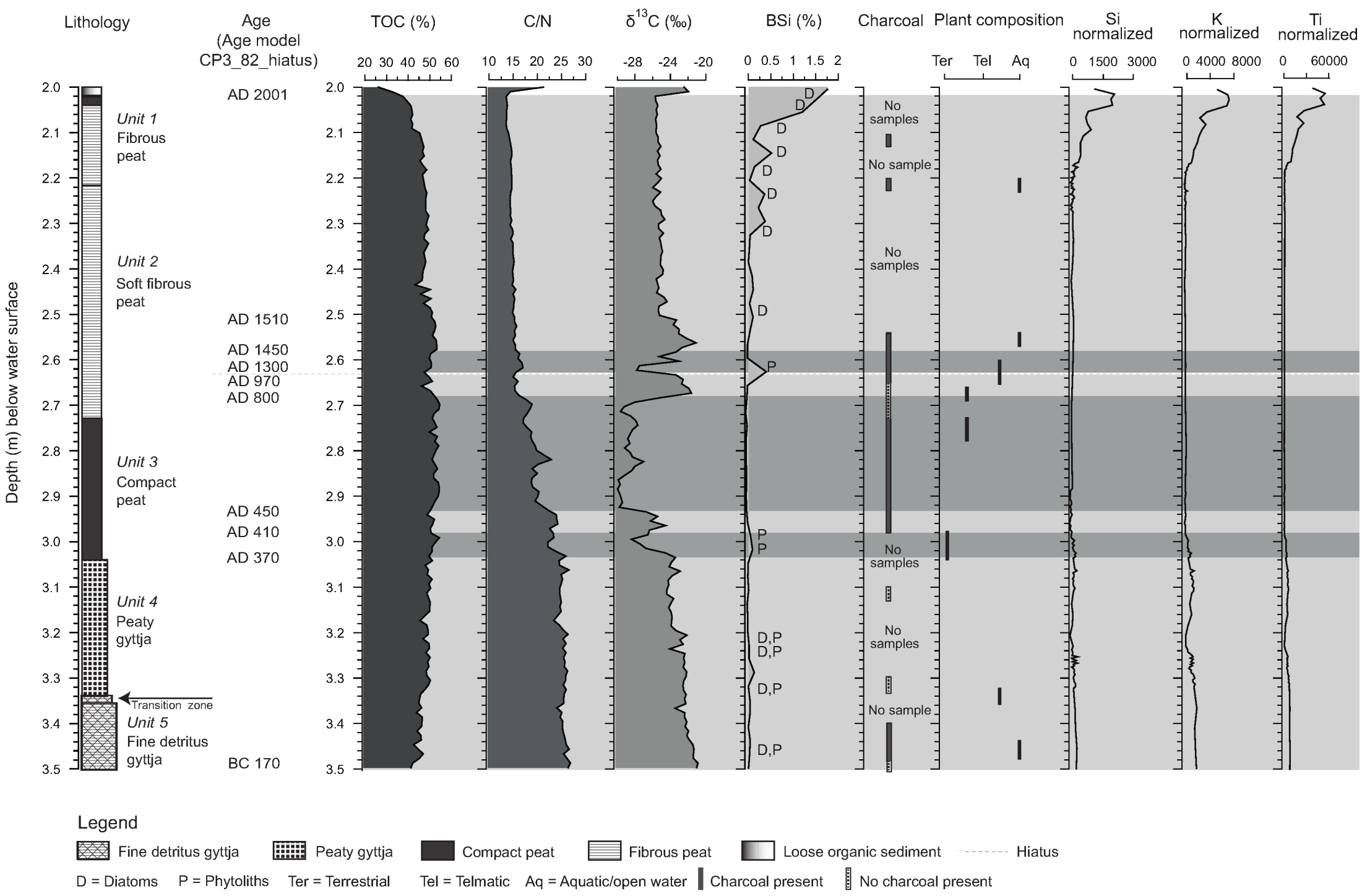
Lithology
Age (Age model CP3_82_hiatus)
TOC (%)
C/N
δ13C (‰)
BSi (%)
Charcoal
Plant composition
Si normalized
K normalized
Ti normalized
Depth (m) below water surface
Unit 1 Fibrous peat
Unit 2 Soft fibrous peat
Unit 3 Compact peat
Unit 4 Peaty gyttja
Transition zone
Unit 5 Fine detritus gyttja
AD 2001
AD 1510
AD 1450
AD 1300
AD 970
AD 800
AD 450
AD 410
AD 370
BC 170
No samples
No sample
Ter Tel Aq
Legend
Fine detritus gyttja
Peaty gyttja
Compact peat
Fibrous peat
Loose organic sediment
Hiatus
D = Diatoms
P = Phytoliths
Ter = Terrestrial
Tel = Telmatic
Aq = Aquatic/open water
Charcoal present
No charcoal present

Figure4

Figure 4

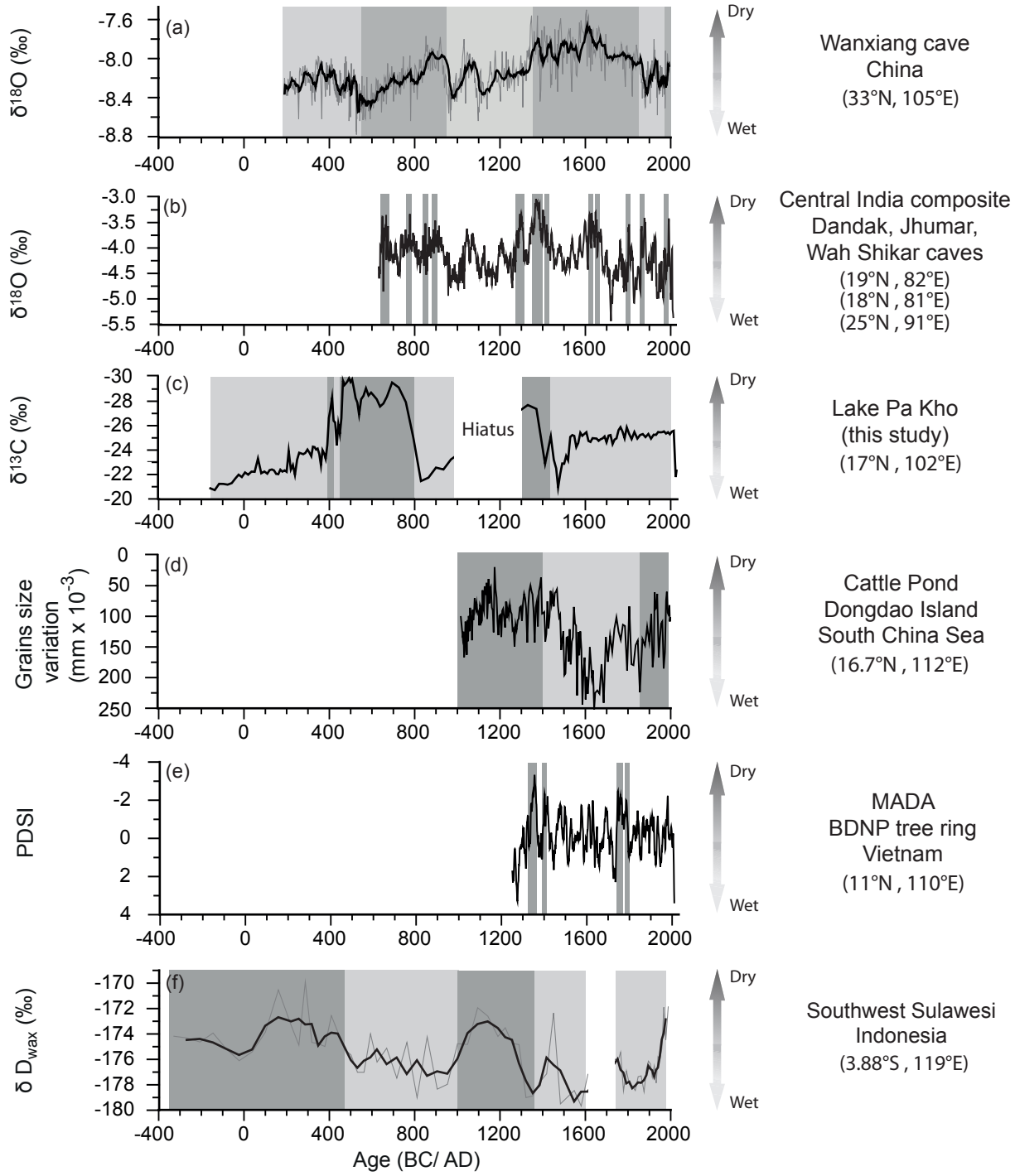

Figure5
Figure 5